RSC Advances

PAPER

View Article Online
View Journal | View Issue

Cite this: *RSC Adv.*, 2015, **5**, 53419

Nano and micro-TiO_2 for the photodegradation of ethanol: experimental data and kinetic modelling

Claudia L. Bianchi,[ad] Carlo Pirola,[ad] Federico Galli,[ad] Marta Stucchi,*[ad] Sara Morandi,[bd] Giuseppina Cerrato[bd] and Valentino Capucci[c]

Received 26th March 2015
Accepted 8th June 2015

DOI: 10.1039/c5ra05385d

www.rsc.org/advances

With TiO_2-photocatalysis being an effective alternative to other more expensive Advanced Oxidation Processes (AOPs), the possibility of using micro-sized TiO_2 materials rather than the well-known nano-sized powders is an important goal in terms of both handling safety and cost saving. In this work the photodegradation of ethanol, used as a model VOC (Volatile Organic Compound) molecule, was investigated, comparing the efficiency of both commercial nano- and micro- sized TiO_2 samples. In all cases the same degradation pathway was observed, namely, a consecutive first-order reaction with acetaldehyde as an intermediate product and CO_2 and water as the final products. All photocatalysts were characterized by means of XRD, TEM, IR, BET and XPS analysis. A kinetic model was also developed considering the collected experimental data and a regression of both adsorption and kinetic constants was made using MATLAB software. The optimized parameters were used for simulating the experimental data using an ode15s algorithm.

1 Introduction

Photocatalysis is a well-known process in which a chemical reaction occurs when a semiconductor is hit by radiation that complies with its band gap. In particular, when the semiconductor is irradiated by a light source with an appropriate wavelength, some of its electrons are transferred from the valence band to the conduction band, creating electron–hole pairs that are capable of causing reduction and oxidation reactions.[1]

TiO_2 is an excellent photocatalyst used for degrading organic compounds, which are oxidized according to the aforementioned mechanism. In particular, UV irradiation induces the formation of electron–hole pairs, whose charge carriers react with chemical species such as water molecules (humidity) and molecular oxygen present in the air to produce hydroxyl radicals ($^{\bullet}OH$) and superoxide radical anions ($O_2^{\bullet -}$), respectively, which contribute to the decomposition of organic molecules at the TiO_2 surface.[1–3]

Chemical stability and also the high oxidizing power of the photogenerated holes are the main characteristics that make TiO_2 the most used and investigated photocatalyst and also the key factors for the pollutant oxidation.[4]

Pollution abatement is something that is very important nowadays, but worldwide research needs to develop new "green" technologies in order to limit energy consumption and save money, and also to take advantage of processes with no environmental drawbacks.[5] In a sense, the TiO_2-photodegradation of pollutants, in particular organic compounds, nitrogen and sulphur oxides, is an effective alternative to the much more expensive advanced oxidation processes (AOPs).[6] Moreover, as most of human life spent in an indoor environment, and most of the soilage of the interior of buildings comes from VOCs, their degradation is a very crucial point in order to improve both air and human health quality.[4,7]

In this study, two different commercial TiO_2 samples were tested in the photodegradation reaction of ethanol, which was chosen as a model molecule. Furthermore, considering it as an important atmospheric pollutant, commonly used as an industrial solvent and a fuel additive, its oxidation is of interest because it is emitted from many industrial processes such as breweries and bakeries. Ethanol emissions accounted for about 4% of the total VOC anthropogenic emissions in the UK in 1993.[8]

Moreover, the atmospheric concentrations of this pollutant are rising as a consequence of the use of ethanol as a biofuel in the automotive sector and it is well established that this fact implies an increase in the atmospheric levels of acetaldehyde, which is far more toxic and reactive in the atmosphere than ethanol.[9,10] Besides this, acetaldehyde, also present in the ethanol photodegradation pathway, is an important indoor pollutant itself, released by some building materials such as polyurethane foams, and some consumer products such as

[a]*Dip. Chimica, Università degli Studi di Milano, via C. Golgi 19, 20133 Milan, Italy. E-mail: marta.stucchi@unimi.it*
[b]*Università di Torino & NIS Inter-departmental Centre, Torino, Italy*
[c]*GranitiFiandre SpA, Castellarano (MO), Italy*
[d]*Consorzio INSTM, Firenze, Italy*

cigarettes, adhesives, coatings and inks.[11] In fact, ethanol is first oxidized to acetaldehyde and then completely degraded to carbon dioxide and water.

The possibility of using the common pigmentary micro-sized TiO_2 as a photocatalyst has already been proved,[12] and, although a reduced crystal size ensures a higher surface area (that is positive in terms of photocatalytic activity), it is a disadvantage in terms of safety and product handling; in fact, nano-powders can be very dangerous for health, as reported in several recent papers.[13,14] A nanomaterial consists of one or more components, present in various forms, that possesses at least a one-dimensional structure with an average diameter in the 1–100 nm range. A quick search through the literature shows that the bulk of the research articles on nanomaterials genotoxicity were published within the past 3 years, even though their cytotoxicity and carcinogenic responses, both *in vitro* and *in vivo*, were assessed previously.[15] As the development of nanotechnological applications continue to grow, it is anticipated that there will be an even greater demand for safety, health and risk assessment studies in the forthcoming years.[16]

In the present paper, two micrometric commercial samples and the well-known nano-sized P25 by Evonik have been chosen with a two-fold aim: *i.e.*, not only to evaluate the semiconductor efficiency, considering the different crystallite sizes, but also to verify the ethanol photodegradation pathway with all the tested materials.

From a kinetic point of view, the whole process can be simplified considering a first reaction on the catalyst surface, in which the adsorbed ethanol is converted to the adsorbed acetaldehyde, followed by a second reaction, in which the adsorbed acetaldehyde is mineralized to carbon dioxide and water, following a Langmuir–Hinshelwood mechanism. The experimental data gathered were used for the regression of the characteristic kinetic parameters, assuming pseudo first order kinetic constants.

2 Experimental

Ethanol is a Fluka product at a high purity grade (99.9%). Three powdered commercial TiO_2 samples were selected without further treatment before their characterization and use: (i) a nanometric sample by Evonik (P25), always used as a photocatalytic reference material and (ii) two micrometric samples (1077 by Kronos and A-HR by Hunsdman), sold as pigments and chosen with the following features: pure anatase, untreated surfaces, an undoped material, and a powdery form.

2.1 Sample characterization

The surface area of all the catalysts was determined by conventional N_2 adsorption (BET) at 77 K using a Sorptometer (Costech Mod. 1042).

X-ray photoelectron spectra (XPS) were taken in an M-probe apparatus (Surface Science Instruments). The source was monochromatic Al Kα radiation (1486.6 eV).

The morphology of the catalysts was inspected by means of high-resolution transmission microscopy (HR-TEM): images were recorded using a JEOL 3010-UHR instrument (acceleration potential: 300 kV; LaB_6 filament).

Absorption/transmission IR spectra were obtained on a Perkin-Elmer FT-IR System 2000 spectrophotometer equipped with a Hg–Cd–Te cryo-detector, working in the 7200–580 cm^{-1} range at a resolution of 2 cm^{-1} (number of scans $\sim$ 20). Before the IR analysis, powdery samples were compressed in self-supporting discs (of about 10 mg cm^{-2}) and placed in a homemade quartz cell, equipped with KBr windows, connected to a conventional high-vacuum line (UHV). The spectra were recorded at room temperature (RT) on the samples in air or after prolonged outgassing at RT.

For the characterization of the light absorption features and band-gap determinations, diffuse reflectance spectra (DRS) of the powders were collected using a UV-vis scanning spectrophotometer (PerkinElmer, Lambda 35), which was equipped with a diffuse reflectance accessory.

The XRD spectra were collected using a PW 3830/3020 X' Pert Diffractometer from PANalytical working Bragg–Brentano, using the Cu Kα_1 radiation ($\lambda = 1.5406$ Å).

2.2 Photocatalytic tests

Photocatalytic degradations were conducted in a cylindrical glass reactor (diameter = 200 mm, volume = 5 L). The amount of catalyst used in each test was 0.05 g and it was deposited on a glass support as a thin film. The latter is obtained by preparing a suspension of isopropanol and TiO_2, and depositing it on the glass slide through a Pasteur pipette.[17] The reactor was initially charged with chromatographic air humidified at 40% RH. The starting ethanol concentration was set at 400 ppmV. Photon sources were provided by a 500 W UV lamp (Jelosil model HG 500) emitting in the 315–400 nm wavelength range (UV-A) at 30 Wm^{-2} on the sample surface and each test lasted 4 h.[18] The ethanol photodegradation was monitored, using on-stream gas chromatography (Agilent 3000 A microGC), directly connected to the reactor, that automatically measures the internal concentration of ethanol, acetaldehyde and carbon dioxide.

Photolysis tests were also performed for both pure ethanol and acetaldehyde to monitor the possible molecule degradation under UV light in the absence of a photocatalyst. The same procedure was repeated using acetaldehyde. Adsorption tests were also carried out by monitoring the concentration for 4 hours for both ethanol and acetaldehyde in the dark to obtain the adsorption constants (K) separately, in order to reduce the model parameters to be estimated. This approach has been already used in the literature for the independent determination of adsorption and kinetic constants.[19,20]

All the photocatalytic tests carried out on each powder have been repeated at least 5 times, exhibiting the same behavior for each run.

The regression of both the adsorption and the kinetic constants were made using MATLAB software, minimizing the sum of the squared errors between the calculated and the experimental data. The optimized parameters were used for simulating the experimental data using a differential equation solver able to handle stiff problems, *i.e.* the ode15s algorithm.[21]

3 Results and discussion

3.1 Morphological characterization

The morphological characteristics of all the used catalysts are reported in Table 1.

XRD analysis confirms the well-known P25 phase composition, 80 : 20 in anatase/rutile ratio, and shows that anatase is the unique polymorph for the other two samples, 1077 and A-HR. One of the most critical drawbacks of both the micrometric samples is their low specific surface area. However, the presence of the bare anatase polymorph is confirmed, and this is a fundamental feature in terms of the photocatalytic performance.

As for the general morphology of the various samples, low magnification TEM images are displayed in Fig. 1. It is evident that P25 totally reveals its nano-sized nature (average particle size $\sim$ 20–30 nm) if compared to both the 1077 and A-HR powders (for which the average particles size is much larger, lying in the 100–180 nm range). The high-resolution images relative to all the samples (see the inset in each image reported in Fig. 1) confirm the high crystallinity exhibited by the powders and the phase composition, as well.

BET surface area data are consistent with the above considerations. In fact, a particle size located in the nano-size range, as in case of P25, implies a much higher surface area and *vice versa* the opposite trend is expected for the micro-sized powders (see Table 1, column 2 and 3).

The surface state of the TiO_2 particles was analyzed by XPS. No significant differences can be observed in the Ti 2p region concerning the binding energies (BEs). The peak Ti $2p_{3/2}$ is always regular and the BE (see Table 1, column 4) compares well with the data for Ti(IV) reported in the literature for TiO_2 materials.[22] The analysis of the oxygen peaks reveals the presence of more than one component, which can be attributed to lattice oxygen in TiO_2 (529.9 eV) and to surface OH species (>531.5 eV).[19]

The hydrophilicity/hydrophobicity characteristics of the photocatalyst surface plays a crucial role in determining the ethanol adsorption and thus the final photocatalytic activity, at least in the degradation of pollutants.[23] The sixth column of Table 1 reports the OH/O_{tot} surface ratio, which refers to a quantitative measure of the hydrophilicity/hydrophobicity of the TiO_2 surface, estimated using XPS (Fig. 2).[23,24] On one hand, P25 material exhibits the lowest OH/O_{tot} ratio, and its better activity is surely related to its higher surface area, which ensures a bigger amount of surface OH groups, as evidenced by the FTIR spectra (see Fig. 2, section B) in the region of absorption bands related to H-bonded and free hydroxyls (these last evidenced by grey box). In particular P25, differently from both the Kronos and AH-R samples, exhibits a larger amount with high heterogeneity of free hydroxyls, the most important species for the degradation reaction.[18] On the other hand, different values of the OH/O_{tot} ratio result in very similar activity in case of both the Kronos 1077 and AH-R powders. This is related to the fact that the XPS analysis gives a result which refers to the entire number of OH groups. The FTIR spectra (Fig. 2, section B) provides evidence for a larger amount of H-bonded OH groups for Kronos 1077, but very similar features of free OH for both the samples.

3.2 Kinetic parameters regression

The degradation reaction is followed considering this pathway:[14]

$$\begin{cases} (1)\ CH_3CH_2OH_{ads} \overset{k_1}{\rightarrow} CH_3COH_{ads} \\ (2)\ CH_3COH_{ads} \overset{k_2}{\rightarrow} 2CO_2 + H_2O \end{cases}$$

Photocatalyzed reactions in which a gas phase reactant is involved are usually interpreted using the Langmuir–Hinshelwood mechanism,[25] where only the reactant molecules previously adsorbed on the catalytic surface take part in the reaction. This kinetic interpretation is well-known for photocatalyzed reactions, as reported in some previous papers.[26,27]

For the regression of the kinetic parameters in the present paper, two consecutive first order reactions were considered, as shown in the scheme reported in the introduction section. The differential equation system that characterizes the system is reported here:

$$\begin{cases} \dfrac{dn_e}{dt} = -k_1 \dfrac{K_e n_e}{1 + K_e n_e + K_a n_a} \\ \dfrac{dn_a}{dt} = +\dfrac{k_1 K_e n_e - k_2 K_a n_a}{1 + K_e n_e + K_a n_a} \\ \dfrac{dn_{CO_2}}{dt} = +2k_2 \dfrac{K_a n_a}{1 + K_e n_e + K_a n_a} \end{cases}$$

K_e and K_a (mol^{-1}) are the adsorption constant for ethanol (e) and acetaldehyde (a), respectively, and k_1 and k_2 (mol min^{-1}) are the first order kinetic constants. As can be observed, the adsorption of CO_2 was not considered.

The adsorption constant (K_i) was obtained considering reversible adsorption for both ethanol and acetaldehyde. The differential equation used for this regression is:

$$\frac{dn_i}{dt} = -k_{ads,\,i} n_i + k_{des,\,i}(n_{0,\,i} - n_i)$$

Table 1 Main features of the selected TiO_2 samples

Sample	Anatase/Rutile composition	BET surface area ($m^2\ g^{-1}$)	Average crystallite size (nm)	XPS Ti $2p_{3/2}$ (eV)	XPS OH/O_{tot}	Band gap (eV)
P25	80% anatase 20% rutile	52	26	458.4	0.14	3.21
1077	100% anatase	11	130	458.4	0.32	3.15
A-HR	100% anatase	12	130	458.0	0.14	3.15

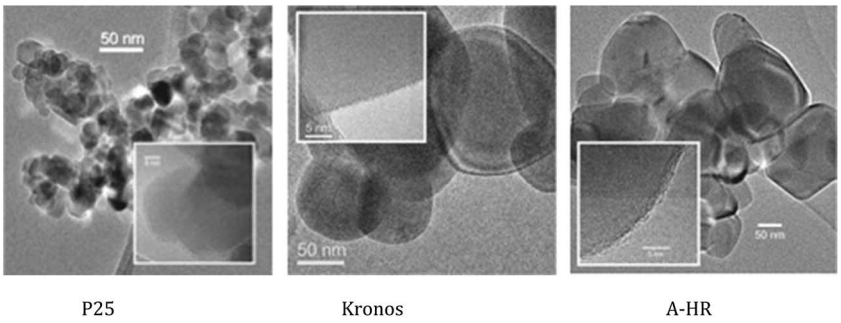

Fig. 1 TEM images of the various TiO_2 samples.

for either ethanol or acetaldehyde, $n_{0,i}$ is the moles of the component charged in the reactor and n_i is the moles of the component at a certain time. The adsorption constant is then calculated by dividing k_{ads} by k_{des} after the regression.

3.3 Photolysis and adsorption tests

In order to determine the real role of the photocatalytic process, both photolysis and simple ethanol absorption were investigated.

The photolysis contribution is negligible, and it can be concluded that both ethanol and its oxidized intermediate product, *i.e.* acetaldehyde, are not sensitive to the bare UV light, and their concentrations remain stable for the entire test.

The role of absorption is different, as displayed in Fig. 3a (P25) and b (Kronos 1077) (AH-R sample gave very similar results to the 1077 adsorption and is not reported for the sake of clarity).

The optimized adsorption constants calculated from these experimental data are reported in Table 2:

The results indicate that P25 possesses a higher adsorption constant for ethanol if compared to that exhibited by both micrometric samples. On the contrary, acetaldehyde results show an opposite trend and the adsorption of these species seems to have no relation with the OH/O surface ratio of the catalyst.

In Fig. 4–6 the experimental data obtained in the photocatalytic runs performed using the different catalysts have been reported, together with the calculated trend using the optimized kinetic parameters.

The regressed kinetic parameters are reported in Table 3:

The simulated results, obtained with the optimized kinetic parameters, exhibit a good fit for the test performed using both P25 and the micrometric samples. This was also confirmed by the low value of the sum of the squared errors (SSE). It is possible to observe the great difference between the nanometric (P25) and micrometric (AHR and 1077) samples. In fact, the numerical values of both the kinetic constants are larger for P25, in agreement with its superior catalytic performance. Moreover, for this sample the k_2 constant is one order of magnitude larger than the corresponding k_1 constant; this means that, using nano-sized catalysts, the degradation of acetaldehyde is very fast with respect to the conversion of ethanol. The situation is completely different when the reactions are catalysed by the micrometric samples. In fact, using these catalysts, both the numerical values of the k_1 and k_2 kinetic constants and the numerical value of the constants between the 1077 and AHR samples are very similar. The

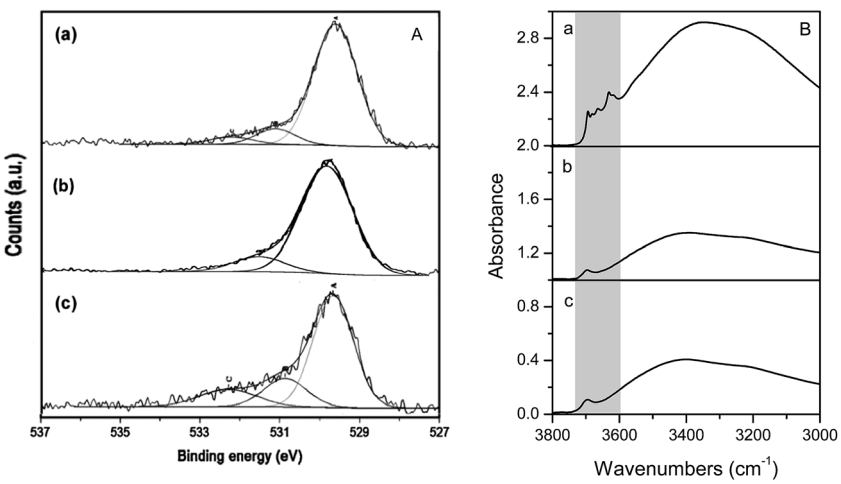

Fig. 2 O_{1s} XPS spectra (A) and FTIR spectra (B) recorded at RT in air for (a) P25, (b) A-HR, (c) 1077.

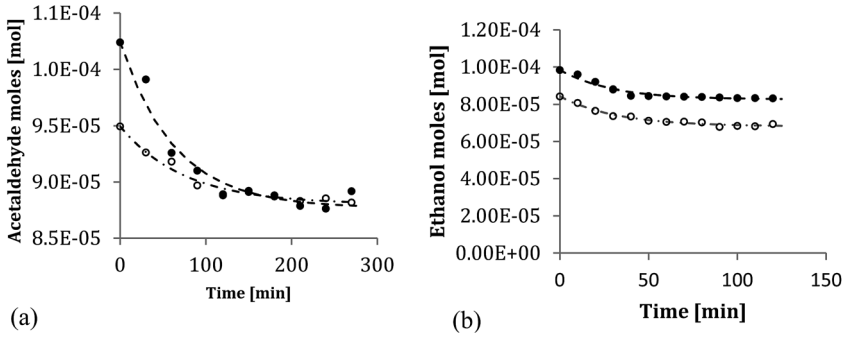

Fig. 3 Adsorption runs of (a) acetaldehyde and (b) ethanol on P25 (○) and 1077 (●). Dotted lines are the calculated curves using the regressed adsorption constants.

Table 2 Adsorption constants regressed from experimental data

	Adsorption constant K [mol^{-1}]		
Component	P25	1077	A-HR
Ethanol	0.2373	0.1891	0.1884
Acetaldehyde	0.0786	0.1680	0.1809

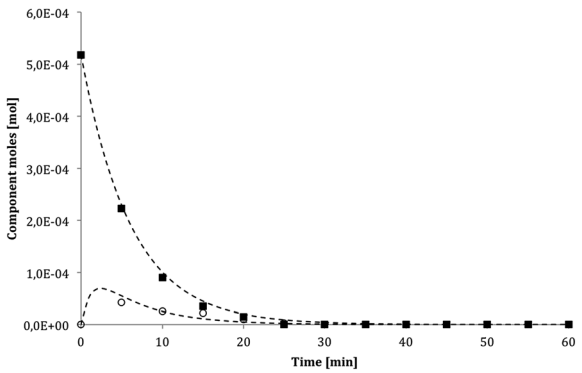

Fig. 4 Experimental ethanol photodegradation tests performed using the P25 catalyst. Empty points represent acetaldehyde. Dotted lines are the simulated trends obtained using the regressed kinetic constant.

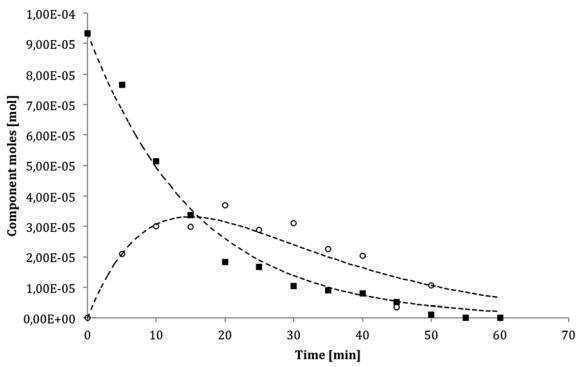

Fig. 5 Experimental ethanol photodegradation tests performed using the 1077 catalyst. Empty points represent acetaldehyde. Dotted lines are the simulated trends obtained using the regressed kinetic constant.

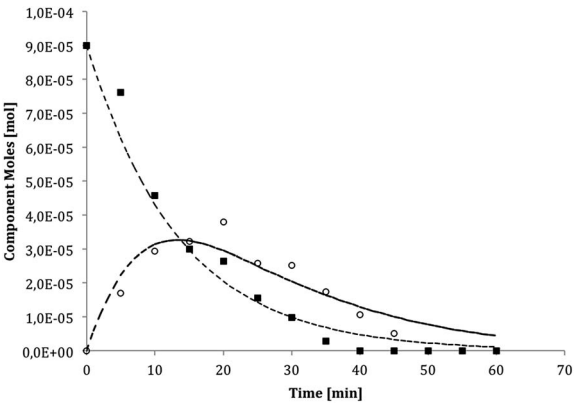

Fig. 6 Experimental ethanol photodegradation tests performed using the A-HR catalyst. Empty points represent acetaldehyde. Dotted lines are the simulated trends obtained using the regressed kinetic constant.

Table 3 Regressed kinetic constant for all the photocatalysts

Sample	k_1 [mol min^{-1}]	k_2 [mol min^{-1}]	SSE
P25	0.68	10.41	3.91×10^{-9}
1077	0.34	0.42	1.69×10^{-9}
AHR	0.39	0.42	6.88×10^{-10}

analysis of the kinetic elaboration gives us important information about the rate of reaction using either the nanometric or micrometric samples. The rate of VOC degradation is in general increased if catalysed by a nanometric sample with respect the micrometric ones. This phenomenon is particularly important for some light compounds (*i.e.*, acetaldehyde). Nevertheless, the catalytic properties of micrometric samples are confirmed from both the direct experimental conversion and this kinetic interpretation. In particular, considering the degradation of ethanol, the rate of its conversion is not so different for either the nanometric or micrometric samples.

The FTIR data obtained for the TiO_2 powders, either before and after the photodegradation processes, indicate that ethanol leaves some residues (traces) onto the surface of the supports, independently of their micro- or nanosized nature. See for

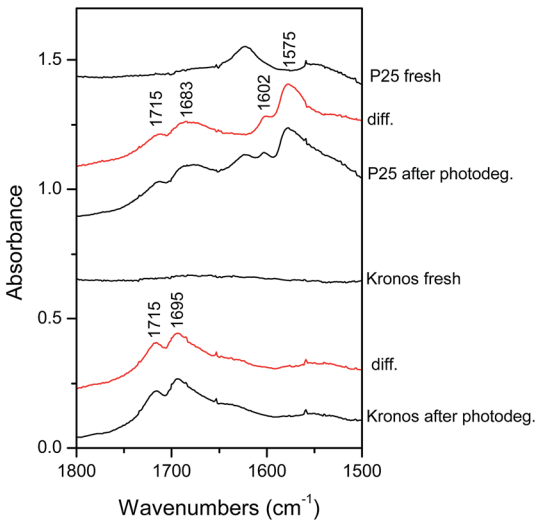

Fig. 7 Absorbance FTIR spectra relative to fresh and used P25 (top spectra) and 1077 (bottom) TiO_2 samples in the ethanol degradation reaction. The differences between the spectra of the samples before and after ethanol degradation are reported in red.

instance Fig. 7, in which we reported the results relative to the nanometric P25 powder (top section of the figure) and to one of the two micrometric materials, namely Kronos 1077 (bottom section of the figure), as the A-HR powder exhibited a trend (almost) coincident to that of Kronos 1077.

In fact, if we refer to the spectral range (1800–1500 cm^{-1}) in which the $\nu_{C=O}$ mode(s) typical of the possible degradation products of ethanol (ketone/aldehyde) are normally located,[28] two net components are evident at ~1715 and ~1695.83 cm^{-1}. This confirms that an effective degradation has occurred, but a few (really only traces) of the degraded products are still present at the surface of the TiO_2 powders. Moreover, for the P25 material, other spectral components located at 1602 and 1575 cm^{-1}, reveal the presence of short chain carboxylated species (namely, acetate/formate species) chemisorbed to the TiO_2 surface. This provides evidence of the formation of acetic acid as an intermediate in acetaldehyde degradation, at least in the case of the nano-sized photocatalyst considered here.

This is also in agreement with the calculated kinetic parameters reported in Table 2. In fact, the P25 material, due to its intrinsic nanometric nature, is confirmed to have the best performance as a photocatalyst, particularly for the degradation of acetaldehyde, as the (k_2) kinetic constant is an order of magnitude larger, if compared to the micrometric samples.

However, considering the bare ethanol degradation, the micrometric samples are able to oxidize it almost completely and thus can be employed for its degradation, being them far less dangerous for human health.

4 Conclusions

The photodegradation of ethanol, as a model for VOCs, was performed using a commercial nanometric sample and two different micrometric powders. As well as presenting this model, the possibility to exploit the photocatalytic potential of the pigmentary TiO_2 is proved, contributing to the already useful photocatalytic processes. The micrometric TiO_2, which is less dangerous and much less expensive with respect to the nanometric P25, is an active photocatalyst, being able to degrade VOCs into CO_2. Also, the rate of reaction and the kinetic constants are lower with respect to P25. The good fitting between the experimental and simulated results confirms the assumption of a consecutive first order reaction mechanism degradation pathway that is not influenced by the TiO_2 crystallite dimension.

Acknowledgements

This research was supported by LIFE+ Environment Policy and Governance project LIFE13 ENV/IT/000140.

References

1 K. Nakata, T. Ochiai, T. Murakami and A. Fujishima, *Electrochim. Acta*, 2012, **84**, 103–111.
2 A. Fujishima, X. Zhang and D. A. Tryk, *Surf. Sci. Rep.*, 2008, **63**, 515–582.
3 K. Nakata and A. Fujishima, *J. Photochem. Photobiol., C*, 2012, **13**, 169–189.
4 A. Fujishima, T. N. Rao and D. A. Tryk, *J. Photochem. Photobiol., C*, 2000, **1**, 1–21.
5 J. Lyu, L. Zhu and C. Burda, *Catal. Today*, 2014, **225**, 24–33.
6 M. Sievers, Advanced Oxidation Processes, *Treatise on Water Science*, 2011.
7 Y. Xu and Y. Zhang, *Atmos. Environ.*, 2004, **38**, 113–119.
8 R. G. Derwent, M. E. Jenkin and S. M. Saunders, *Atmos. Environ.*, 1996, **30**, 181–199.
9 E. M. Martins, S. M. Correa and G. Arbilla, *Atmos. Environ.*, 2003, **37**, 23–29.
10 M. Colón, J. D. Pleil, T. A. Hartlage, M. L. Guardani and M. H. Martins, *Atmos. Environ.*, 2001, **35**, 4017–4403.
11 D. Meroni, S. Ardizzone, G. Cappelletti, C. Oliva, M. Ceotto, D. Poelman and H. Poelman, *Catal. Today*, 2011, **161**, 169–174.
12 C. L. Bianchi, C. Pirola, F. Galli, G. Cerrato, S. Morandi and V. Capucci, *Chem. Eng. J.*, 2014, **261**, 76–82.
13 S. Bakand, A. Hayes and F. Dechsakulthorn, *Inhalation Toxicol.*, 2012, **24**, 35–125.
14 M. A. Albrecht, C. W. Evans and C. L. Raston, *Green Chem.*, 2006, **8**, 417–432.
15 B. Trouiller, R. Reliene, A. Westbrook, P. Solaimani and R. H. Schiestl, *Cancer Res.*, 2009, **69**, 8784–8789.
16 N. G. Cheng-Teng, J. J. Li, B. H. Bay and L. Y. L. Yung, *J. Nucleic Acids*, 2010, **2010**, 947859, DOI: 10.4061/2010/947859.
17 C. L. Bianchi, C. Pirola, E. Selli and S. Biella, *J. Hazard. Mater.*, 2012, **211–212**, 203–207.
18 C. L. Bianchi, S. Gatto, C. Pirola, A. Naldoni, A. Di Michele, G. Cerrato, V. Crocellà and V. Capucci, *Appl. Catal., B*, 2014, **146**, 123–130.
19 T. Popken, L. Gotze and J. Gmehling, *Ind. Eng. Chem. Res.*, 2000, **39**, 2601–2611.

20 W. Song, G. Venimadhavan, J. M. Manning, M. F. Malone and M. F. Doherty, *Ind. Eng. Chem. Res.*, 1998, **37**, 1917.
21 L. F. Shampine and M. W. Reichelt, *SIAM J. Sci. Comput.*, 1997, **18**, 1–22.
22 G. Cappelletti, C. L. Bianchi and S. Ardizzone, *Appl. Surf. Sci.*, 2006, **253**, 519–524.
23 S. Ardizzone, C. L. Bianchi, G. Cappelletti, A. Naldoni and C. Pirola, *Environ. Sci. Technol.*, 2008, **42**, 6671–6676.
24 S. Ardizzone, C. L. Bianchi, G. Cappelletti, S. Gialanella, C. Pirola and V. Ragaini, *J. Phys. Chem. C*, 2007, **111**, 13222–13231.
25 C. S. Turchi and D. F. Ollis, *J. Catal.*, 1990, **122**, 178–192.
26 M. L. Sauer and D. F. Ollis, *J. Catal.*, 1996, **158**, 570–582.
27 I. K. Konstantinou and T. A. Albanis, *Appl. Catal., B*, 2004, **49**, 1–14.
28 L. H. Little, *Infrared Spectra of Adsorbed Species*, Academic Press, London, 1966.